Accepted Manuscript

Title: Gold-TiO$_2$-Nickel catalysts for low temperature–driven CO oxidation reaction

Author: Mariana Hinojosa Reyes Rodolfo Zanella Viridiana Maturano Rojas Vicente Rodríguez González

Please cite this article as: M.H. Reyes, R. Zanella, V.M. Rojas, V.R. González, Gold-TiO$_2$-Nickel catalysts for low temperaturendashdriven CO oxidation reaction, *Applied Surface Science* (2016), http://dx.doi.org/10.1016/j.apsusc.2016.01.285

Gold-TiO$_2$-Nickel catalysts for low temperature–driven CO oxidation reaction

Mariana Hinojosa Reyes[a*], Rodolfo Zanella[b*], Viridiana Maturano Rojas[b], Vicente Rodríguez González[a]

[a]División de Materiales Avanzados, IPICYT, Instituto Potosino de Investigación Científica y Tecnológica, Camino a la Presa San José 2055 Col. Lomas 4a. sección C.P. 78216, San Luis Potosí, S.L.P., México.

[b]Centro de Ciencias Aplicadas y Desarrollo Tecnológico, Universidad Nacional Autónoma de México, Circuito Exterior S/N, Ciudad Universitaria, A. P. 70-186, Delegación Coyoacán, C.P. 04510, México D. F. México.

E-mail: kittyhinojosa@hotmail.com, rodolfo.zanella@ccadet.unam.mx

Graphical abstract
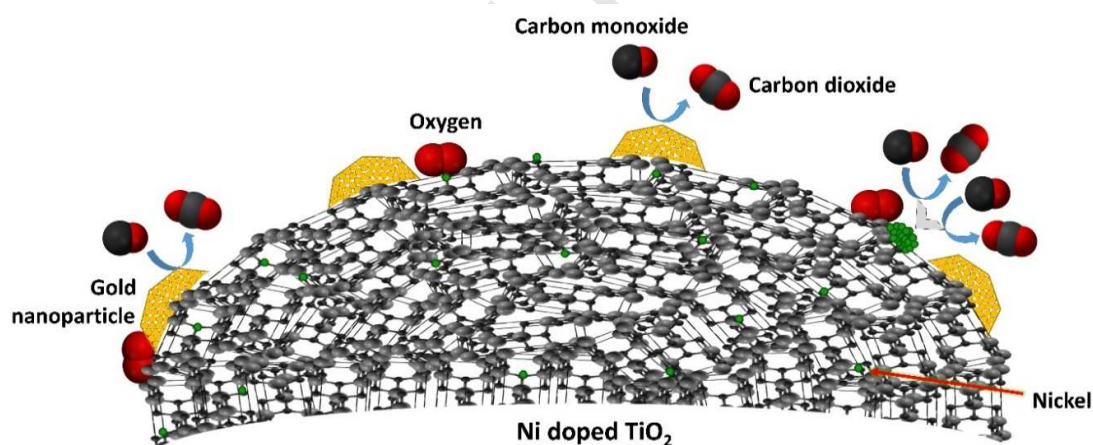
Abstract

Nickel-doped-TiO$_2$ catalysts were prepared by the sol-gel method and surface modified with gold nanoparticles (AuNPs) by the urea-deposition-precipitation technique. The as-synthesized catalysts were characterized by X-ray diffraction, Raman and XPS spectroscopies, N$_2$ physisorption, STEM-HAADF microscopy and TPR hydrogen consumption. The Au/TiO$_2$-Ni catalysts were evaluated catalytically performing CO

1

oxidation reactions. The catalyst with nickel content of 1 wt. % (Au/TiO$_2$-Ni 1) showed the highest CO conversion with respect to the high-nickel-content or bare/commercial TiO$_2$ at 0 °C. *In situ* DRIFTS showed a strong participation of both nickel due to the presence of surface-nickel-metallic nanoparticles formed during the CO adsorption process at reaction temperatures above 200 °C, and surface-bridged-nickel-CO species. A minor deactivation rate was observed for the Au/TiO$_2$-Ni 1 catalyst in comparison with the Au/TiO$_2$ one. The oxygen vacancies that were created on the sol-gel-doped TiO$_2$ improved the catalytic behavior during the performance of CO oxidation reactions, and inhibited the AuNP sintering.

Keywords

CO oxidation, Gold nanoparticles, Nickel-doped TiO$_2$, DRIFTS, Low temperature oxidation.

Highlights

- Nickel-doped TiO$_2$ catalysts (1 wt. %) drive the CO oxidation at low temperature.
- DRIFTS reveals the participation of nickel during the CO oxidation.
- Ni(CO)$_2$ bridged species are detected by DRIFTS.
- Au/TiO$_2$-Ni 1 is the most active and stable catalyst with respect to undoped TiO$_2$.
- Ti^{3+} species corroborate Ni doped TiO$_2$ and surface oxygen vacancies.

1. Introduction

Historically, bulk gold had been considered as inert until the end of the 80´s when Haruta *et al*. discovered that nanometric gold (2 – 3 nm) supported on metallic oxides shows a high catalytic activity for CO oxidation either at room or lower temperatures [1]. From this discovery, gold nanoparticles (AuNPs) have been supported on different metal oxides to perform different catalytic environmental reactions such as propylene epoxidation [2], water – gas shift [3], water splitting [4], etc. The high affinity of AuNPs for carbon monoxide is due

2

to the mixing of gold d-orbitals within the carbon monoxide HOMO level, which is different from bulk gold, where there is a large gap between the d-band center and Fermi level that leads to large Pauli repulsions [5]. The most widely studied catalyst for CO oxidation is gold supported on TiO_2 because it is one of the most active catalysts for carrying out this reaction at low temperature [6]. TiO_2 has been selected for its reducible properties as well as Fe_2O_3 or NiO which usually exhibit appreciably better catalytic performances than non-reducible oxides such as MgO, Al_2O_3 or SiO_2. Reducible supports are beneficial to this reaction because they facilitate the O_2 activation [7]. Other factors that affect the performance of the CO oxidation reaction are the size and preparation method of the AuNPs; as for the first factor, larger particles promote the creation of misfit dislocations and the surface lattice constant will approach the bulk metal value [8], and the second factor affects dispersion [9].

In this work, the use of Ni doped TiO_2 is proposed due to the reducible properties of both TiO_2 and nickel, and similar ionic radii of nickel and titanium atoms. Nickel oxide has been reported as a catalyst for hydrogenation reactions, Wolff-Kishner and Clemmensen reduction, Fisher Tropsch methanation, among other reactions [10, 11], and also for the photocatalytic hydrogen production from methanol either using NiO supported on TiO_2 [12] or nickel titanate nanotubes [13]. For the CO oxidation reaction, nickel has been used as nanosized nickel ferrite powders ($NiFe_2O_4$), where lower crystal sizes (~8.5 nm) enhanced the CO adsorption and consequently its oxidation [14]; as for nonstoichiometric nickel-manganese spinel oxides, they have shown to be highly reactive for CO oxidation, even at room temperature [15]; in the case of NiO and CuO-NiO supported on ceria-alumina mixed oxides, they have exhibited a good catalytic activity during the CO oxidation at subzero temperature, where this high activity is attributed to the formation of well-dispersed and highly reducible metal oxide CuO-NiO species over the mixed oxide support [16]. Comsup *et al.* [17] claimed that the Ti^{3+} presence on the larger crystallite size TiO_2 stabilizes the small Ni particles

3

during the impregnation, calcination, and reduction steps via stronger metal – support interactions, having higher CO oxidation activities and lower light-off temperatures. Therefore, based on the good catalytic properties of nickel, this metal was used in the present research work as a doping agent to improve the structural and surface properties of TiO_2.

The novelty of this work resides in the first-time use of nickel doped TiO_2 as a support of gold nanoparticles to catalyze the CO oxidation reaction. The doping of TiO_2 with elements whose oxidation state is lower than 4+ promotes the creation of surface oxygen vacancies (SOVs); therefore, these SOVs could act as fixing centers for the AuNPs, stabilizing their size to avoid their evolution. On the other hand, the redox properties of nickel enhance the oxygen activation during the CO oxidation reaction. Finally, in the same context, surface nickel can adsorb CO and enhance its oxidation reaction, obtaining high CO conversion rates at low temperatures with respect to bare TiO_2 [18].

2. Experimental section

2.1. Sol – gel nickel doped TiO_2 synthesis

Sol-gel-Ni-TiO_2 catalysts were prepared by a controlled sol-gel process using titanium (IV) isopropoxide (Sigma-Aldrich, 97%) as titanium precursor and nickel nitrate hexahydrate (II) (Sigma-Aldrich, 97%) as doping agent precursor; ethanol (Le Cap Group, 96%) and distilled water were used as solvents. According to a previously reported sol-gel synthesis [19], first, an appropriate amount of nitrate salt was dissolved in water to obtain Ni loadings between 0.5 and 5.0 wt. %. The Ni-TiO_2 catalyst was prepared by adding dropwise 75.6 mL of titanium isopropoxide and 22.9 mL of ethanol-18 mL of water; the nickel solution was added to a 22.9 mL ethanol–18 mL water solution contained in a 4-neck round bottom flask (1 L) equipped with magnetic stirrer and thermometer. The alkoxide/ethanol/water molar ratio was 1/3/8. Later on, the solution was vigorously stirred at 50°C during the addition of the reagents. Subsequently,

4

the solution was gradually heated up to 70 °C. The gelled product was aged for 48 h at 70°C. The solvents and unreacted precursors were removed at 80 °C and dried overnight under vacuum at 100 °C. Finally, the materials were thermally treated at 500 °C for 4 h at a rate of 2 °C min^{-1}. The materials were identified as TiO_2-Ni X, where X indicates the nickel loading (wt. %).

2.2. Synthesis of AuNPs by the urea deposition-precipitation method

Supported AuNPs (2 wt. %) were prepared in the absence of light since it is known that light decomposes and reduces the gold precursors [20]. The preparation of the AuNPs was performed by the urea deposition-precipitation method (DPU) [20]. The gold precursor, $HAuCl_4$ (4.2 10^{-3} M), and urea (0.42 M) were dissolved in 49.29 mL of distilled water; the initial pH of the solution was 2.4. Then, two grams of the support were added to this solution under constant stirring; thereafter, the suspension temperature was increased up to 80 °C and kept constant for 16 h. The urea decomposition led to a gradual rise in pH from 2.4 to 7 [20]. The amount of gold in the solution corresponded to a maximum gold loading of 2 wt. % on the supported catalyst.

After the DPU procedure, all the samples were centrifuged, washed with water at 50 °C and then centrifuged four times and dried under vacuum for 2 h at 100 °C. The thermal treatments for catalyst characterization were performed in a U reactor with a fritted plate of 1.5 cm of diameter; the thermal treatment under hydrogen or air flow (1 mL·min^{-1}mg$_{sample}^{-1}$) was performed at 300 °C for 2 h. All the samples were stored at room temperature under vacuum in a desiccator away from light in order to prevent any alteration [21].

5

2.3. CO oxidation test

The CO oxidation reaction was studied in a flow reactor at atmospheric pressure and increasing the temperature from -5 to 400 °C (light off test). 50 mg of dried catalyst were first activated *in situ* in either a flow of 40 mL·min^{-1} of hydrogen or air with a heating rate of 2 °C/min up to the final chosen temperature, between 300 and 400 °C, followed by a 2-h temperature plateau. After this treatment, the sample was cooled down to -5 °C under the same gas. The reactant gas mixture (1 vol. % CO and 1 vol. % O_2 balanced with N_2) was introduced with a total flow rate of 100 mL/min, and a heating rate of 2 °C·min^{-1}.

The reactor output gases were analyzed with an Agilent Technologies 6890N online gas chromatograph equipped with a FID detector, a methanizer and a HP Plot Q column.

The stability of the catalysts vs. time on stream was examined at 10 °C for a 24-h run, using 50 mg of catalyst activated *in situ* in air at the same heating rate and temperature plateau as described above.

2.4. Characterization techniques

The thermally treated samples were characterized by X-ray diffraction in order to identify crystalline phases using a Bruker Advance 8 Diffractometer with CuKα radiation (1.5404 Å); the crystalline phases were corroborated with Raman spectroscopy, using a Micro-Raman Renishaw spectrometer equipped with an argon laser (514 nm).

After *ex situ* thermal treatment under the same conditions as for the carbon monoxide oxidation (300 °C/H_2) reaction, the samples were examined by transmission electron microscopy in a Tecnai FEI 300 transmission electron microscope (TEM) operated at 300 kV. The samples were suspended in isopropanol and then sonicated for 5 min. Finally, the samples were mounted on a Cu TEM grid. The particle size distribution histograms for the catalysts were obtained from the measurements of about 200 particles. The average particle

6

diameter (d_s) was calculated using the following formula: $d_s = \Sigma n_i d_i / \Sigma n_i$, where n_i is the number of particles of diameter d_i.

The specific surface area was calculated by the Brunauer–Emmett–Teller method (BET method) on a Quantachrome Autosorb 1. The hydrogen temperature programmed reduction (H_2-TPR) study of the dried materials was performed in a RIG-150 unit under a flow of 10 % H_2/Ar gas mixture (30 mL min^{-1}) with a heating rate of 10 °C min^{-1} from room temperature to 200 °C. H_2O produced during the reduction process was trapped before the TCD detector.

The XPS experiments were performed for the samples thermally treated *ex situ* at 300 °C under H_2 atmosphere in a K-Alpha spectrometer by Thermo Scientific using monocromatic radiation Kα of Al at 1486.68 eV.

CO adsorption was followed by FTIR spectroscopy to characterize the metallic surface. The experiments were carried out in a Nicolet 670FT-IR spectrophotometer equipped with a Praying Mantis for DRIFT spectroscopy and a low/high temperature reaction chamber by Harrick. In each experiment, approximately 25 mg of dried sample were packed in the sample holder and pretreated *in situ* under H_2 flow (30 mL·min^{-1}, heating rate of 2 °C·min^{-1}) up to the chosen temperature followed by a 1-h plateau. After the thermal treatment, the sample was cooled down to room temperature under the same gas flow and then purged with N_2 before the introduction of 5 % of CO in N_2 (30 mL·min^{-1}). A spectrum recorded under N_2 was used as a reference, and then several spectra were recorded under the CO flow until the band intensity was stable; afterwards, the temperature was increased under CO, and the spectra were recorded at increasing temperatures. After DRIFTS experiments, the samples were recovered and analyzed by TEM microscopy.

3. Results and discussion

3.1. Physicochemical properties of Au/TiO$_2$-Ni catalysts

7

In Figure 1, X-ray diffractograms for nickel doped and undoped TiO_2 are shown. All the catalysts show the formation of anatase as main crystalline phase (JCPDS 04-002-2678); as for commercial Evonik P25, it additionally shows the rutile crystalline phase (JCPDS 70-7347; 80 % anatase and 20 % rutile) and for the sol-gel-nickel-doped TiO_2, at contents higher than 1 wt. %, the formation of a rhombohedral nickel titanate ($NiTiO_3$) crystalline phase (JCPDS 04-012-0745) by segregation is observed. Both tetragonal anatase and nickel titanate could coexist [22]. Additional peaks related to other crystalline phases of Ni and Ti were not detected.

Using the FWHM of the crystallographic plane (101) of anatase and Scherrer equation, the crystallite size was determined, see Table 1. The crystallite size shows a decrease as the nickel content increases due to the fact that nickel retards the anatase crystallite growth [23], and nickel starts to segregate through the TiO_2 surface forming the $NiTiO_3$ phase.

The surface area values of the catalysts are presented in Table 1. The sol-gel catalysts show surface area values above 70 m^2/g, being the Au/TiO_2-Ni the one that shows the highest value with almost 80 m^2/g, while Au/P25 features a surface area of 51 m^2/g.

Raman spectroscopy was carried out to corroborate the crystalline phases. Figure 2 shows the vibrational modes corresponding to the anatase crystalline phase: E_g – 144 cm^{-1}, E_g – 197 cm^{-1}, B_{1g} – 400 cm^{-1}, $A_{1g} + B_{1g}$ – 515 cm^{-1} and E_g – 640 cm^{-1} [24], in addition, two vibrational modes of $NiTiO_3$ are tagged in Figure 2b [25].

By analyzing the main Eg vibrational mode (Figure 2a), the doping of the catalysts can be inferred since the spectrum of bare TiO_2 shows a FWHM peak located at 143.9 cm^{-1}, while the spectra of TiO_2 loaded with 1 and 5 wt. % show a peak displacement toward 145.2 and 146.1 cm^{-1}, respectively. This shift is meaningful because this vibrational mode is associated with O-Ti-O bending vibrations in the TiO_2 frame, which suggests a shortening or rigidity of

8

this chemical bond, which is mainly due to the increase in surface oxygen vacancies attributed to the incorporation of Ni into the TiO_2 structure, which reduces the O/Ti rate [26]. TPR profiles are shown in Figure 3. This technique was used to elucidate the reduction temperature of gold and the effect of the nickel-TiO_2 support on these temperatures. As it is well known, after the DPU process (before the thermal treatment), the oxidation state of gold nanoparticles is III, which directly comes from the $HAuCl_4$ precursor [27]. Figure 3 shows the reduction peaks located between 90 and 180 °C with maxima located at 141.9, 144.9, 114.2 and 158.5 °C for Au/P25, Au/TiO_2, Au/TiO_2-Ni 1 and Au/TiO_2-Ni 5, respectively. These reduction peaks have been attributed to the reduction of Au(III) to Au^0 species; the TiO_2 P25 thermogram was also carried out, but no reduction peak was detected within this temperature interval [28]. As gold reduction depends on the support, the low reduction temperature for a nickel content of 1 wt. % could be related to the increase in the number of TiO_2 surface defects. It has been previously shown that defective structures caused by dopants with oxidation states below (+4) introduced in oxides create vacancies that lead to higher lattice oxygen mobility which enhances the reduction processes [18]. In addition, due to redox nickel oxide properties, this element could donate electrons to enhance the gold reduction. On the other hand, the high reduction temperature for a nickel content of 5 wt. % at 158.1 °C indicates a strong interaction between the gold nanoparticles and the support which probably stems from the interaction between Au NPs and nickel and / or nickel titanate crystals.

The catalysts thermally treated at 300 °C, under hydrogen atmosphere, were analyzed by transmission electron microscopy in the STEM-HAADF mode. Images are shown in Figure 4, where the AuNPs correspond to brilliant and white dots. In the three catalysts, a homogenous dispersion of AuNPs is observed in both AuNP sizes and space distributions, and the average gold particle size is located at around 2 to 3 nm in all cases.

9

In order to analyze the surface chemical composition of the as-prepared catalysts, XPS experiments were carried out. Figure 5 shows the comparison of Au/TiO$_2$-Ni 1 and Au/TiO$_2$ samples, which were thermally treated at 300 °C under H$_2$ atmosphere.

In Figure 5a, the titanium spectra for Au/TiO$_2$ show the characteristic binding energies located at 464.5 and 458.7 eV, which correspond to the photoelectronic splitting of 2p$_{1/2}$ and 2p$_{3/2}$ orbitals [29]. The Au/TiO$_2$-Ni 1 spectrum shows a shift to higher binding energies, 464.8 and 459.1 eV. This shift toward higher energies implies that the local chemical state is slightly influenced by Ni^{2+} incorporation into the TiO$_2$ lattice [30]. Figure 5a-b shows the Ti deconvoluted XPS spectra. As for Au/TiO$_2$, only the contribution of Ti^{4+} is detected while for the doped Au/TiO$_2$-Ni 1 sample, the contribution of Ti^{4+} and Ti^{3+} are detected. This information corroborates the presence of nickel doped TiO$_2$ because Ti^{3+} is directly associated with surface oxygen vacancies caused by nickel incorporation into the TiO$_2$ lattice [31].

The photoelectronic splitting of gold in the Au/TiO$_2$ sample shows binding energies located at 87.1 and 83.4 eV related to 4f$_{5/2}$ and 4f$_{7/2}$ orbitals, respectively (Figure 5d) while for the Au/TiO$_2$-Ni 1 sample, the same photoelectronic splitting is observed at higher binding energies, 87.6 and 84.0 eV. The binding energies are shifted about 0.5 eV with respect to Au/TiO$_2$, indicating a charge transfer from the TiO$_2$ surface to gold [32]. The deconvolution of both spectra originated four sub-bands, two well defined related to Au^0 and two shoulders related to Au^{3+}. According to the area of the deconvolution peaks for each species, a rate of Au^{3+}/Au^0 of 0.19 was found for Au/TiO$_2$, which corresponds to 16.1 % of Au^{3+}. For the case of Au/TiO$_2$-Ni 1, a Au^{3+}/Au^0 rate of 0.17, corresponding to 14.8 % of Au^{3+} was found. A small fraction of Au^{3+} species may be present in the interface between the AuNPs and Ni-TiO$_2$ support [33]. However, it is important to note that it has also been reported [21] that for Au/TiO$_2$ samples, the oxidation state of gold can be altered when they are analyzed by XPS

10

because of the ultrahigh vacuum and photon beam. This fact could explain the differences observed in the results obtained by XPS and TPR.

The nickel XPS spectra show a characteristic $2p_{3/2}$ orbital with a binding energy of 856.3 eV and another sub-band at 862.1 eV (Figure 5g); additionally, at 873.9 eV, a $2p_{1/2}$ orbital band with a sub-band at 881.2 eV is observed. The separation of 17.65 eV among these orbitals reveals the presence of Ni^{2+}, which corresponds to the oxidation state of Ni^{2+} in the nickel titanate framework [34].

3.2. Catalytic activity in the CO oxidation reaction

Initially, the effect of the *in situ* thermal treatment conditions on the CO oxidation reaction was studied using the Au/TiO$_2$-Ni 1 catalyst (Figure 6). According to the light off test curves, at 0°C, a CO conversion of 75 % was observed after a thermal treatment of 300 °C under hydrogen while with the same thermal treatment, but under air atmosphere, the CO conversion was 25 % while it was 35 % for the sample thermally treated at 400 °C under air. Therefore, an *in situ* thermal treatment at 300 °C under hydrogen seems to produce the highest CO conversion. These differences in catalytic activity displayed by the Au/TiO$_2$ catalysts when activated in hydrogen or in air atmosphere are due to differences in particle size, morphology, chloride content and interaction with the support as a function of the activating gas [21, 35]; on the other hand, when Au/TiO$_2$ catalysts are treated in air, the gold particles are larger than when they are treated in hydrogen; moreover, a thermal treatment with H$_2$ can remove chlorides from the support surfaces as hydrochloric acid [21].

Based on the previous experiments, we proceeded to evaluate the rest of the catalysts using a thermal treatment at 300 °C under hydrogen atmosphere. Figure 7, reveals the behavior of these catalysts. Au/TiO$_2$-Ni 1 shows the highest CO conversion (75 % at 0 °C), and the rest of the catalysts show a similar behavior, reaching 50 % of CO conversion at about 35 °C,

11

even for the Au/TiO$_2$ (P25) reference. Therefore, the optimal nickel load was 1 wt. %. It is important to mention that the TiO$_2$-Ni bare support did not show CO conversion under identical reaction conditions [3]. Thus, the catalytic activity of Au/TiO$_2$-Ni 1 is remarkably high in comparison with the rest of the synthesized catalysts, which is likely due to a weak interaction between gold and nickel that leads to high electron combinations which enable oxidation reactions; in addition, this behavior could be due to the creation of surface oxygen vacancies that stabilize the gold nanoparticles [18]. This means that in Au/TiO$_2$-Ni 1, the interaction between the nickel doped support and AuNPs drives the CO oxidation at low temperature. The less active catalyst was Au/TiO$_2$-Ni 5 whose behavior was probably due to the nickel titanate formation whose non reducible properties and strong interaction between nickel titanate and gold cause a decrement in the catalytic activity during the CO oxidation reaction. The highest activity of the Au/TiO$_2$-Ni 1 catalyst can be due to the fact that gold shows the lowest temperature reduction (114.2 °C) with respect to the rest of the catalysts (142 to 159 °C), indicating that the reaction takes place at lower temperatures due to its oxidation-reduction properties, and the increase in the number of TiO$_2$ surface defects, which determine the behavior in the CO oxidation reaction.

The CO conversion of the most active catalyst (Au/TiO$_2$-Ni 1, thermally treated at 300 °C under hydrogen atmosphere) was studied as a function of the reaction time at 10 °C to know its temporal stability, see Figure 8. The Au/TiO$_2$-Ni 1 catalyst shows a slight deactivation of 19 %, where this deactivation is lower than the one above 50 % observed for the Au/TiO$_2$ catalyst previously reported by us, evaluated at the same reaction temperature and under the same reaction conditions [36]; in this sense and for comparative purposes, Figure 8 shows the stability of our sample (Au/TiO$_2$-Ni) and that of the one previously reported (Au/TiO$_2$) [36]. In another study, an Au/TiO$_2$(P25) catalyst evaluated at 15 °C lost about 60 % of its initial

12

activity after 24 h under the same reaction conditions [37]. Therefore, nickel doped TiO_2 enhances the stability due to the fact that the surface oxygen vacancies stabilize the AuNPs.

Surface characterization by in situ DRIFTS

In order to understand the surface chemistry of the catalysts, DRIFTS experiments were carried out during the CO adsorption – desorption processes using the Au/TiO_2-Ni 1 catalyst thermally treated at 300 °C under hydrogen atmosphere. Figure 9a shows that the adsorption equilibrium at room temperature was reached after 30 minutes. For this spectrum series, a band at 2107 cm^{-1}, which is displaced to 2116 cm^{-1} as a function of time, is observed; this band is associated with molecular CO adsorbed onto the Ti surface of TiO_2 [38]. An important increase in the band at 2067 cm^{-1} (between 0 and 30 minutes) is also observed due to the constant reduction of Au^0 to $Au^{\delta-}$ and to the fact that the CO absorption has higher affinity for $Au^{\delta-}$ than for Au^0 [39].

The CO desorption by temperature increase is shown in Figure 9b. The decrease in the intensity bands and their shift toward lower wavenumbers due to physical desorption phenomena are observed. The shift of the $Au^{\delta-}$-CO band is due to the decrease in the dipole-dipole interaction which occurs because the gold surface CO coverage decreases when temperature increases [40]. At 300 °C, a new band located at 2013 cm^{-1}, attributed to the lineal adsorption of CO on metallic nickel, appears [41], suggesting that there are nickel crystals that grow on the TiO_2 surface at high reaction temperatures (300 °C). Another significant change occurs with the formation of a band at 1896 cm^{-1} at temperatures between 50 and 200 °C; this band is associated with bridged carbonyls on cationic sites, namely $Ni(CO)_2$ [42]. Nevertheless, at temperatures up to 250 °C, this band disappears due to a physical desorption process (Figure 9b) while in the Au/TiO_2 reference, this band does not occur due to the absence of nickel.

13

Additionally, the Au/TiO$_2$-Ni 1 catalyst was analyzed by transmission electron microscopy, after the DRIFTS experiment, to corroborate the evolution of the AuNP sizes due to the temperature changes and also to the CO adsorption-desorption process (Figure 10). The gold particle size increased from 2.3 to 2.7 nm, which explains in part the deactivation observed in Figure 8.

Figure 11 shows a schematic representation of the Au/TiO$_2$-Ni catalysts under the reaction conditions. The TiO$_2$ lattice is represented by black (oxygen) and gray (titanium) spheres; the doping Ni is represented by intercalated green spheres; nickel nanoparticles are represented by green cumulus, and gold nanoparticles are represented by yellow icosahedral clusters of gold atoms. The adsorption of CO mainly occurs at low coordinated sites of gold nanoparticles and on the surface nickel oxide crystals forming bridged species, while oxygen could be adsorbed and activated at the periphery between the AuNPs and Ni-TiO$_2$ support.

4. Conclusions

Raman spectroscopy corroborated the TiO$_2$ nickel doping due to a Raman shift in the main vibrational mode (Eg) of anatase, suggesting the formation of surface oxygen vacancies which diminish the O/Ti rate. Nickel doping was also confirmed by the presence of Ti^{3+} detected by XPS. These surface and structural changes in doped TiO$_2$ allowed the AuNP stabilization, promoting the CO oxidation reaction at 0 °C with CO conversion of 82% for the Au/TiO$_2$-Ni 1 catalyst. Additionally, nickel plays a major role during the CO oxidation reaction due to the formation of Ni(CO)$_2$ bridged species and also to the formation of nickel metallic particles at reaction temperatures above 300 °C. It is important to mention that the presence of nickel in the Au/TiO$_2$-Ni 1 catalyst also enhanced the stability during the reaction with respect to the undoped Au/TiO$_2$ during the deactivation test.

14

References

[1] M. Haruta, N. Yamada, T. Kobayahsi, S. Iijima, Gold catalysts prepared by coprecipitation for low-temperature oxidation of hydrogen and of carbon monoxide, J. Catal. 115 (1989) 301 – 309.

[2] T. Hayashi, K. Tanaka, M. Haruta, Selective vapor-phase epoxidation of propylene over Au/TiO$_2$ catalysts in the presence of oxygen and hygrogen, J. Catal. 178 (1998) 566 – 575.

[3] M. Hinojosa Reyes, R. Zanella, V. Rodríguez-González, Gold nanoparticles supported on TiO$_2$-Ni as catalysts for hydrogen purification via water-gas shift reaction, RSC Adv. 4 (2014) 4308 – 4316.

[4] A. Fujishima, K. Honda, Electrochemical photolysis of water at a semiconductor electrode, Nature. 238 (1972) 37 – 38.

[5] N. S. Phala, G. Klatt, E. van Steen, A DFT study of hydrogen and carbon monoxide chemisorption onto small gold clusters, Chem. Phys. Lett. 395 (2004) 33 – 37.

[6] R. Zanella, S. Giorgio, C-H Shin, C. R. Henry, C. Louis, Characterization and reactivity in CO oxidation of gold nanoparticles supported on TiO$_2$ prepared by deposition-precipitation with NaOH and urea, J. Catal. 222 (2004) 357 – 367.

15

[7] L. Delannoy, N. Weiher, N. Tsapatsaris, A. M. Beesley, L. Nchari, S. L. M. Schroeder, C. Louis, Reducibility of supported gold (III) precursors: influence of the metal oxide support and consequences for CO oxidation activity, Top. Catal. 44 (2007) 263 – 273.

[8] M. Mavrikakis, P. Stoltze, J. K. Norskov, Making gold less noble, Catal. Lett. 64 (2000) 101 – 106.

[9] A. Wolf, F. Schüth, A systematic study of the synthesis conditions for the preparation of highly active gold catalysts, Appl. Catal. A. 226 (2002) 1 – 13.

[10] C. A. Brown, V. K. Ahuja, Catalytic hydrogenation. VI. Reaction of sodium borohydride with nickel salts in ethanol solution. P-2 Nickel, a highly convenient, new, selective hydrogenation catalyst with great sensitivity to substrate structure, J. Org. Chem. 38 (1973) 2226 – 2230.

[11] C. H. Herr, F. C. Whitmore, R. W. Schiessler, The Wolff-Kishner reaction at atmospheric pressure, J. Am. Chem. Soc. 67 (1945) 2061 – 2063.

[12] J. Bandara, C. P. K. Udawatta, C. S. K. Rajapakse, Highly stable CuO incorporated TiO_2 catalyst for photocatalytic hydrogen production from H_2O, Photochem. Photobiol. Sci. 4 (2005) 857 – 861.

[13] J. Yu, Y. Hai, B. Cheng, Enhanced photocatalytic H_2-production activity of TiO_2 by $Ni(OH)_2$ cluster modification, J. Phys. Chem. C. 115 (2011) 4953 - 4958.

[14] M. M. Rashad, O. A. Fouad, Synthesis and characterization of nano-sized nickel ferrites from fly ash for catalytic oxidation of CO, Mater. Chem. Phys. 94 (2005) 365 – 370.

[15] C. Laberty, C. Marquez-Alvarez, C. Drouet, P. Alphonse, C. Mirodatos, CO oxidation over nonstoichiometric nickel manganite spinels, J. Catal. 198 (2001) 266 – 276.

[16] B. M. Reddy, K. N. Rao, P. Bharali, Copper promoted cobalt and nickel catalysts supported on ceria – alumina mixed oxide: structural characterization and CO oxidation activity, Ind. Eng. Chem. Res. 48 (2009) 8478 – 8486.

16

[17] N. Comsup, J. Panpranot, P. Praserthdam, Effect of TiO_2 crystallite size on the activity of CO oxidation, Catal. Lett. 133 (2009) 76 – 83.

[18] R. Zanella, V. Rodríguez-González, Y. Arzola, A. Moreno-Rodríguez, Au/Y-TiO_2 catalyst: High activity and long-term stability in CO oxidation, ACS Catal. 2 (2012) 1 – 11.

[19] M. Hinojosa-Reyes, V. Rodríguez-González, S. Arriaga, Enhancing ethylbenzene vapor degradation in a hybrid system based on photocatalytic oxidation UV/TiO_2-In and a biofiltration process, J. Hazard. Mater. 209-210 (2012) 365-371.

[20] R. Zanella, S. Giorgio, C. R. Henry, C. Louis, Alternative methods for the preparation of gold nanoparticles supported on TiO_2, J. Phys. Chem. B. 106 (2002) 7634-7642.

[21] R. Zanella, C. Louis, Influence of the conditions of thermal treatments and of storage on the size of the gold particles in Au/TiO_2 samples, Catal. Today. 107-108 (2005) 768 – 777.

[22] K. Kakegawa, J. Mohri, S. Shirasaki, K. Takahashi, Sluggish pansition between tetragonal and rhombohedral phases of $Pb(Zr,Ti)O_3$ prepared by application of electric field, J. Am. Ceram. Soc. 65 (1982) 515 – 519.

[23] Y. Chen, X. Zhou, X. Zhao, X. He, X. Gu, Crystallite structure, surface morphology and optical properties of In_2O_3-TiO_2 composite thin films by sol-gel method, Mater. Sci. Eng. B. 151 (2008) 179 – 186.

[24] T. Ohsaka, F. Izumi, Y. Fujiki, Raman spectrum of anatase, TiO_2. J. Raman Spectrosc. 7 (1978) 321 – 324.

[25] G. Busca, G. Ramis, J. M. Gallardo-Amores, V. Sánchez Escribano, FT Raman and FTIR studies of titanias and metatitanate powders, J. Chem. Soc., Faraday Trans. 1. 90 (1994) 3181 – 3190.

[26] J. Zhu, J. Ren, Y. Huo, Z. Bian, H. Li, Nanocrystalline Fe/TiO_2 visible photocatalyst with a mesoporous structure prepared via a nonhydrolytic sol-gel route, J. Phys. Chem. C. 111 (2007) 18965 – 18969.

17

[27] A. Sandoval, A. Aguilar, C. Louis, A. Traverse, R. Zanella, Bimetallic Au-Ag/TiO_2 catalyst prepared by deposition-precipitation: High activity and stability in CO oxidation, J. Catal. 281 (2011) 40 – 49.

[28] A. Aguilar-Tapia, R. Zanella, C. Calers, C. Louis, L. Delannoy, Synergistic effects of Ir-Au/TiO_2 catalysts in the total oxidation of propene: influence of the activation conditions, Phys. Chem. Chem. Phys. 2015. DOI: 10.1039/c5cp00590f.

[29] C. D. Wagner, W. M. Riggs, L. E. Davis, J. F. Moulder, G. E. Muilenberg. Handbook of X-Ray photoelectron spectroscopy. Perkin Elmer Corporation. U. S. A. 1979.

[30] J. Zhu, Z. Deng, F. Chen, J. Zhang, H. Chen, M. Anpo, J. Huang, L. Zhang, Hydrothermal doping method for preparation of Cr^{3+}-TiO_2 photocatalysts with concentration gradient distribution of Cr^{3+}, Appl. Catal. B. 62 (2006) 329 – 335.

[31] J. Xia, N. Masaki, K. Jiang, S. Yanagida, Deposition of a thin film of TiO_x from a titanium metal target as novel blocking layers at conducting glass/TiO_2 interfaces in ionic liquid mesoscopic TiO_2 dye-sensitized solar cells, J. Phys. Chem. B. 110 (2006) 25222 – 25228.

[32] Wu, J. Zhang, L. Xiao, F. Chen. Preparation and characterization of TiO_2 photocatalysts by Fe^{3+} doping together with Au deposition for the degradation of organic pollutants, Appl. Catal. B. 88 (2009) 525 – 532.

[33] M. P. Casaletto, A. Longo, A. Martorana, A. Prestianni, A. M. Venezia, XPS study of supported gold catalysts: the role of Au^0 and $Au^{\delta+}$ species as active sites, Surf. Interface Anal. 38 (2006) 215 – 218.

[34] G. Yang, W. Chang, W. Yan, Fabrication and characterization of $NiTiO_3$ nanofibers by sol-gel assited electrospinning, J. Sol-Gel Sci. Technol. 69 (2014) 473 – 479.

18

[35] X. Bokhimi, R. Zanella, A. Morales, V. Maturano, C. Ángeles-Chávez, Au/Rutile catalysts: Effect of the activation atmosphere on the gold-support interaction, J. Phys. Chem. C. 115 (2011) 5856-5862.

[36] A. Gómez-Cortés, G. Díaz, R. Zanella, H. Ramírez, P. Santiago, J. M. Saniger. Au-Ir/TiO$_2$ prepared by deposition precipitation with urea: improved activity and stability in CO oxidation, J. Phys. Chem. C. 113 (2009) 9710 – 9720.

[37] R. Zanella, V. Rodríguez-González, Y. Arzola, A. Moreno-Rodríguez, Au/Y-TiO$_2$ catalyst: High activity and long-term stability in CO oxidation, ACS Catal. 2 (2012) 1–11.

[38] C. Vignatti, M. S. Avila, C. R. Apesteguía, T. F. Garetto, Catalytic and DRIFTS study of the WGS reaction on Pt-based catalysts, Int. J. Hydrogen Energy. 35 (2010) 7302 – 7312.

[39] F. Boccuzzi, A. Chiorino, M. Manzoli, D. Andreeva, T. Tabakova, FTIR study of the low-temperature water-gas shift reaction on Au/Fe$_2$O$_3$ and Au/TiO$_2$ catalysts, J. Catal. 188 (1999) 176 – 185.

[40] E. Roze, P. Gravejat, E. Quinet, J. L. Rousset, D. Bianchi, Impact of the reconstruction of gold particles on the heats of adsorption of linear CO species adsorbed on the Au sites of a 1% Au/Al$_2$O$_3$ catalyst, J. Phys. Chem. C. 113 (2009) 1037 – 1045.

[41] A. Bandara, S. Dobashi, J. Kubota, K. Onda, A. Wada, K. Domen, C. Hirose, S. S. Kano, Adsorption of CO and NO on NiO(111)/Ni(111) surface studied by infrared-visible sum frequency generation spectroscopy, Surf. Sci. 387 (1997) 312 – 319.

[42] K. I. Hadjiivanov, G. N. Vayssilov, Characterization of oxide surfaces and zeolites by carbon monoxide as an IR probe molecule, Adv. Catal. 47 (2002) 307 – 511.

19

Figure captions

Figure 1. Indexed X-ray diffractograms of the TiO_2-Ni catalysts.

Figure 2. Raman spectra of: a) Eg shift vibrational mode, and b) the rest of vibrational modes of TiO_2-Ni catalysts.

Figure 3. Temperature programmed reduction of Au/TiO_2-Ni catalysts.

Figure 4. TEM images in STEM-HAADF mode of Au/TiO_2-Ni catalysts and their corresponding frequency histograms.

Figure 5. XPS analysis of a) comparison of the Ti 2p orbital of Au/TiO_2 and Au/TiO_2-Ni 1 catalysts. Deconvoluted spectra of Ti 2p orbital of b) Au/TiO_2 and c) Au/TiO_2-Ni 1; d) comparison of the Au 4f orbital of Au/TiO_2 and Au/TiO_2-Ni 1 catalysts. Deconvoluted spectra of Au 4f orbital of e) Au/TiO_2 and f) Au/TiO_2-Ni 1; g) deconvoluted spectra of Ni 2p orbital of the Au/TiO_2-Ni 1 catalyst.

Figure 6. *In situ* thermal treatment effect during the CO oxidation reaction using the Au/TiO_2-Ni 1 catalyst.

Figure 7. Au/TiO_2-Ni catalysts *in situ* thermally treated at 300 °C under H_2 atmosphere during the CO oxidation reaction.

Figure 8. Deactivation test during the CO oxidation reaction carried out at 10 °C and with *in situ* thermal treatment at 300 °C under H_2 atmosphere. Au/TiO_2 (*PW*) corresponds to a previously reported sample.

Figure 9. DRIFTS spectra during the a) CO adsorption as a function of time, and b) desorption by increasing temperature from 50 to 300 °C of the Au/TiO_2-Ni 1 catalyst thermally treated at 300 °C under hydrogen atmosphere.

Figure 10. STEM-HAADF image and frequency histogram of the AuTiO_2-Ni catalyst after the DRIFTS experiment.

Figure 11. Schematic representation of the CO oxidation reaction on the Au/TiO_2-Ni catalyst. The green dots correspond to nickel atoms.

Figure 1

20
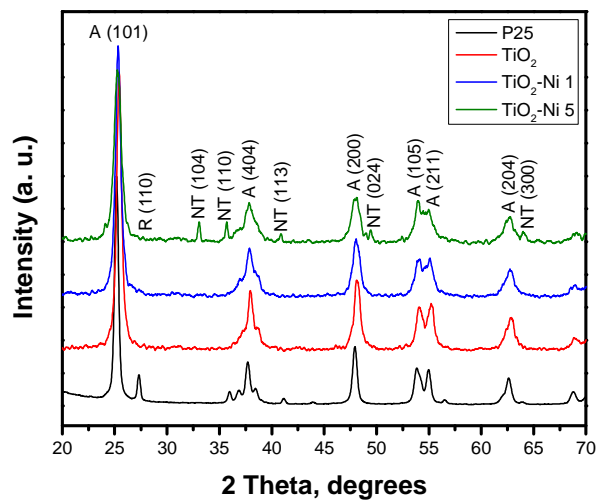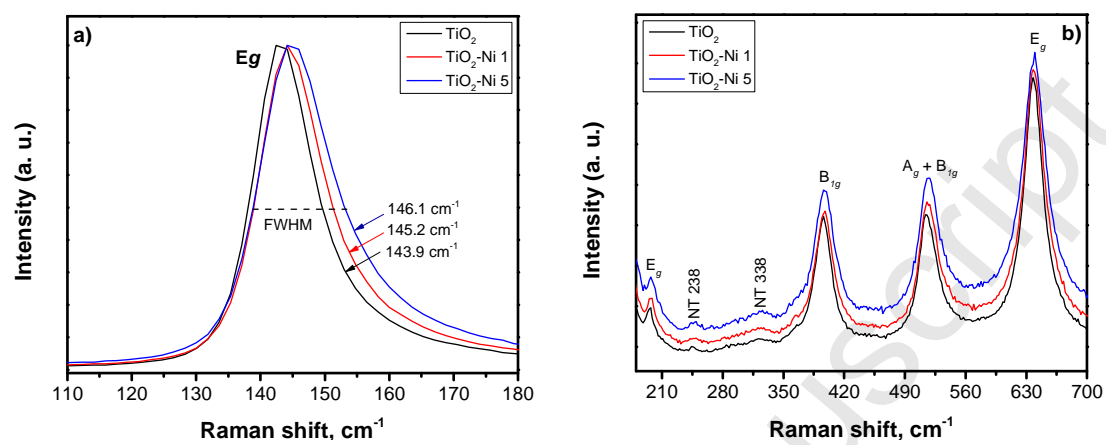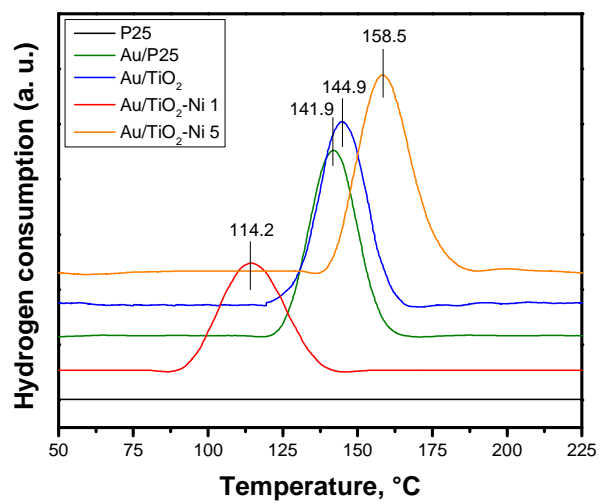
Figure 2

Figure 3

Figure 4
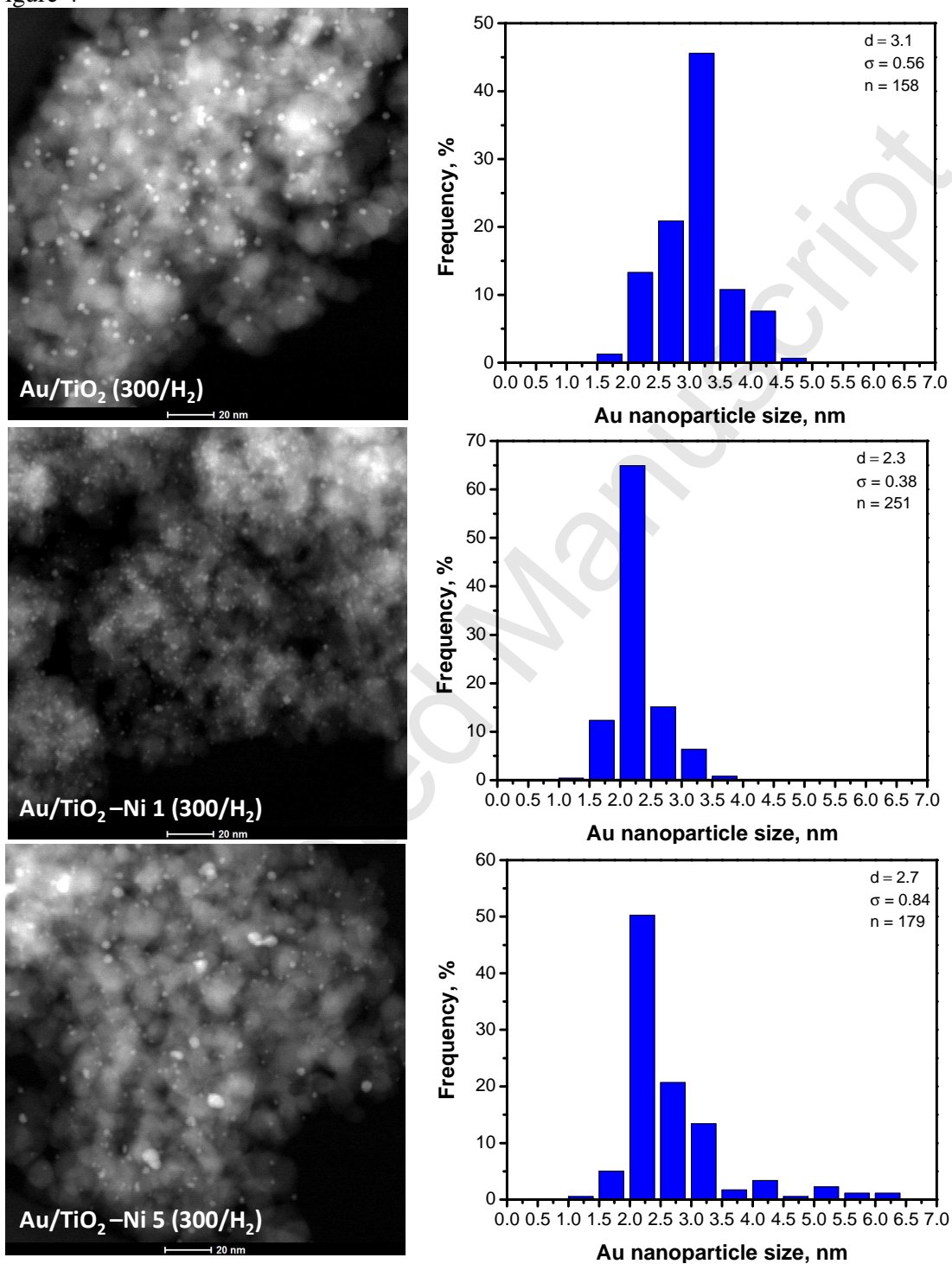
Figure 5
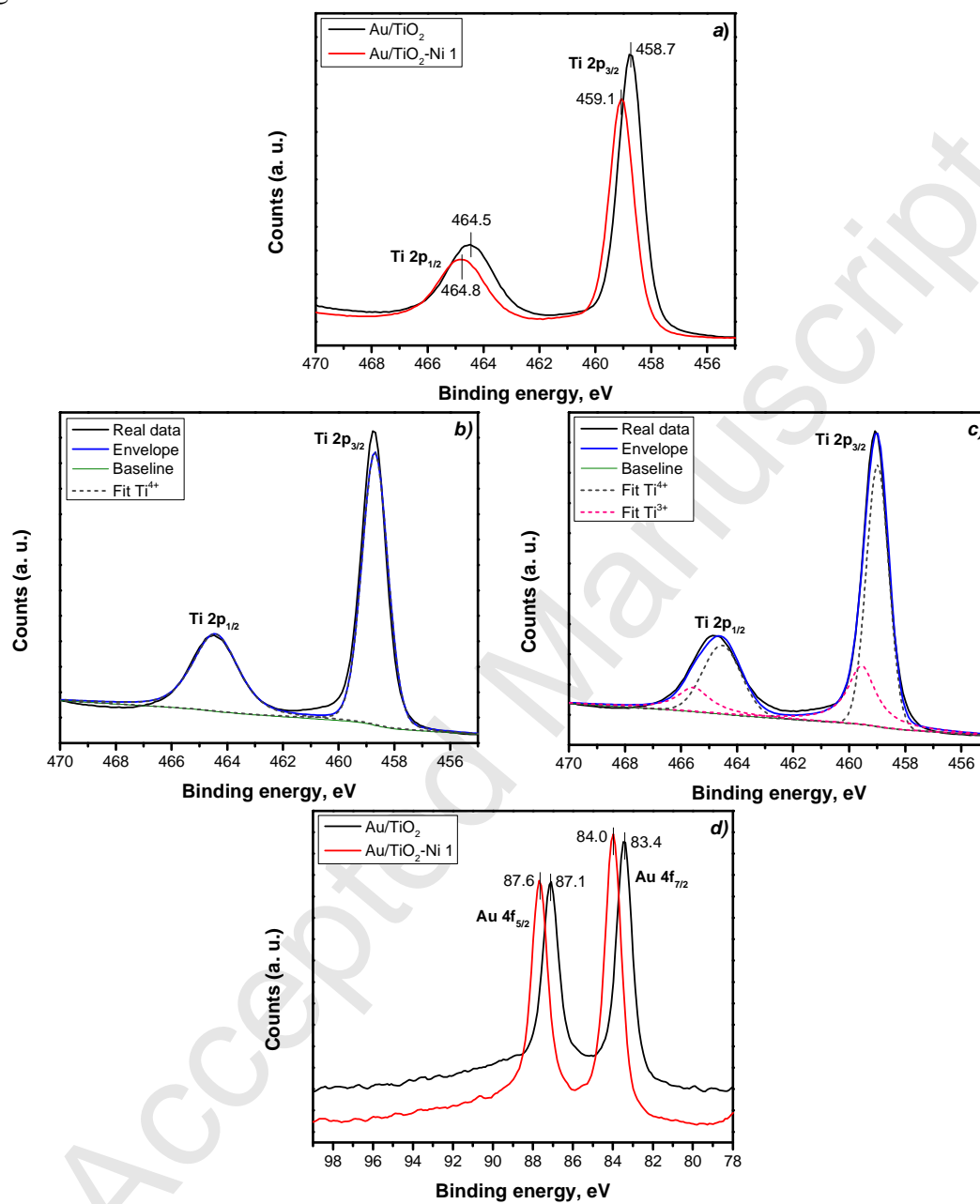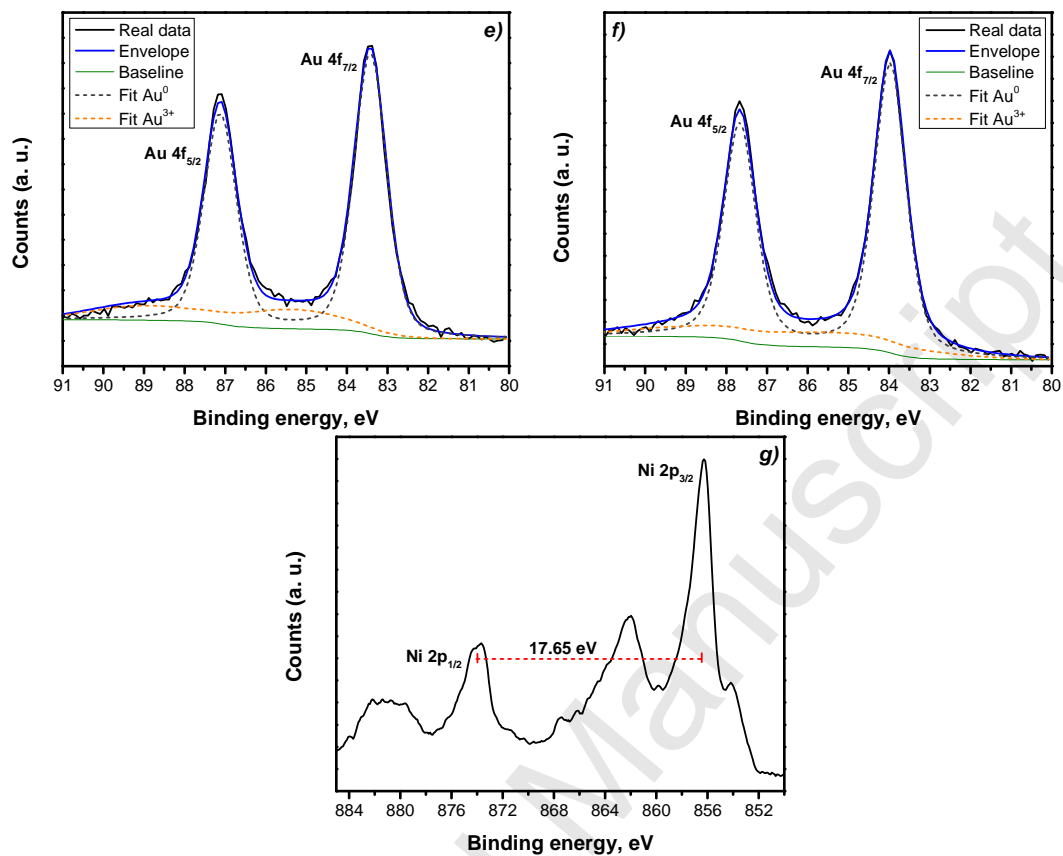
Figure 6
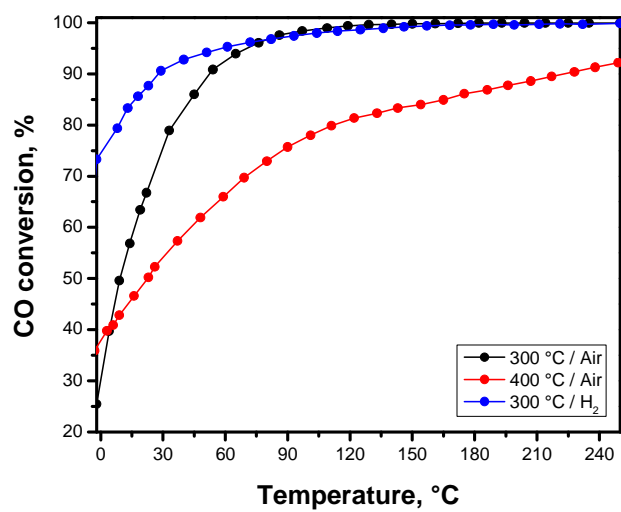
Figure 7
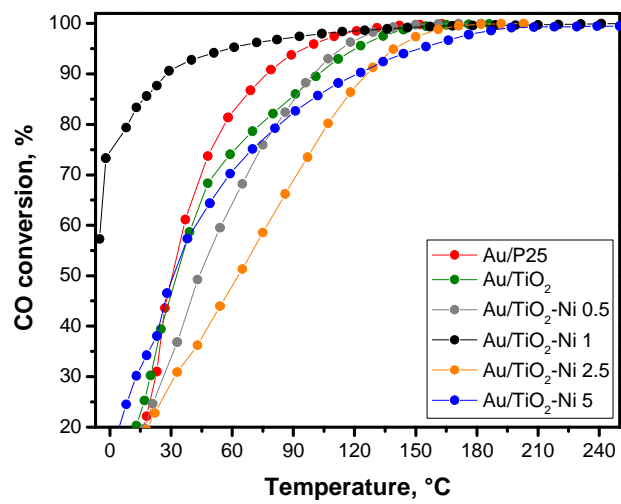
Figure 8

Figure 9

Figure 10

31
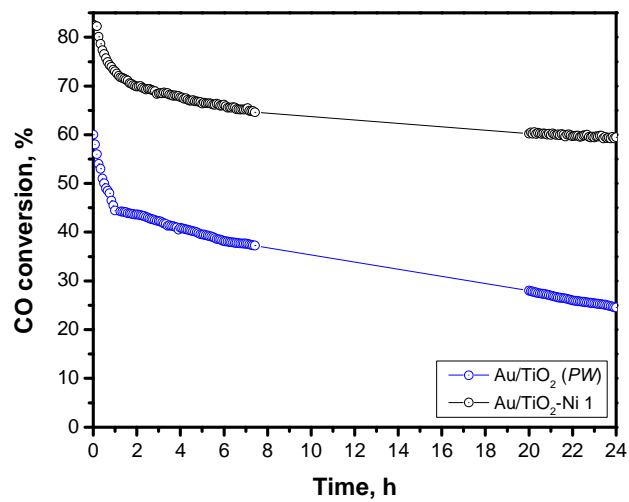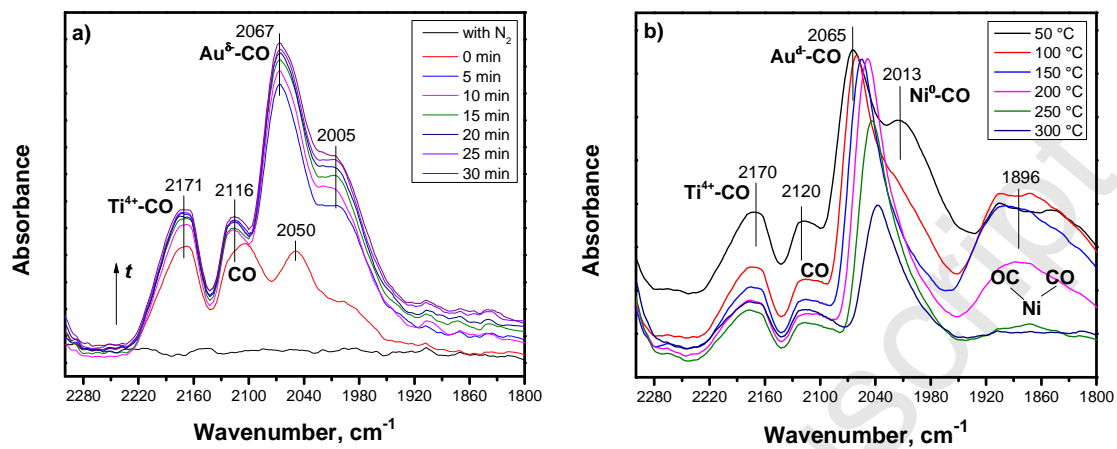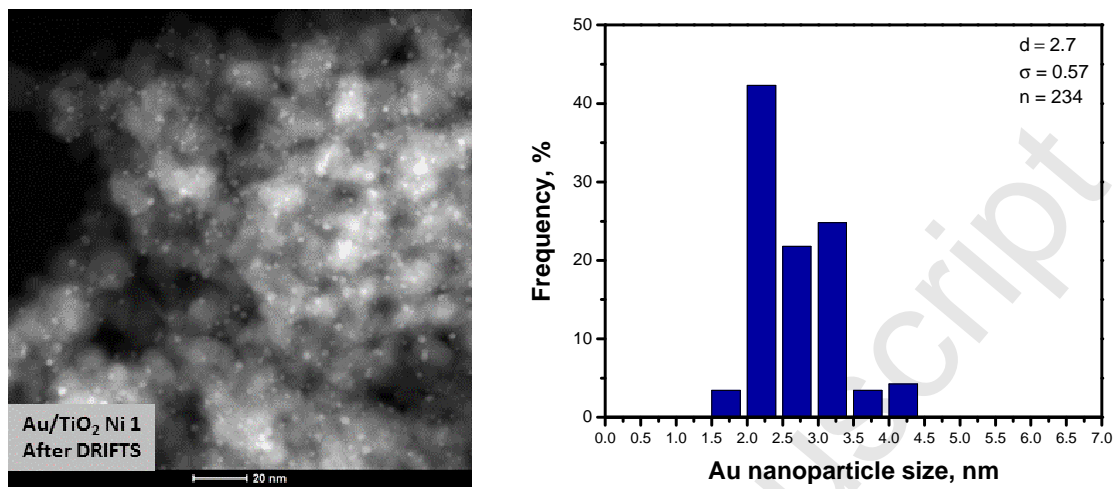
Figure 11
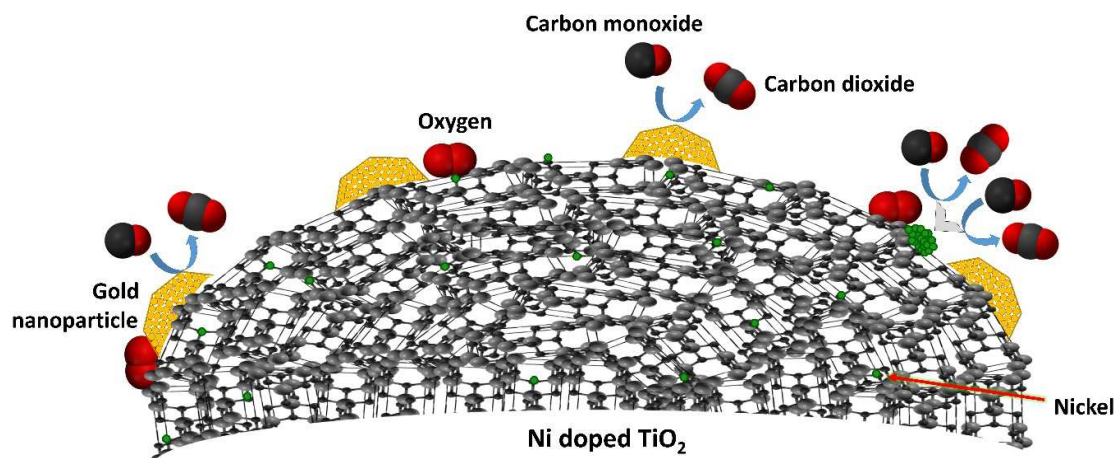
Table 1. Physicochemical properties of the studied catalysts.

	Crystallite size (nm)	Surface area ($m^2\,g^{-1}$)	AuNP size (nm)
Au/P25	19.7	51.3	ND*
Au/TiO$_2$	16.3	72.7	3.1
Au/TiO$_2$-Ni 1	13.9	79.0	2.3
Au/TiO$_2$-Ni 5	10.9	76.3	2.7

*Not available data

32